Pergamon

Cement and Concrete Research 32 (2002) 269–278

CEMENT AND CONCRETE RESEARCH

# Effects of an early or a late heat treatment on the microstructure and composition of inner C-S-H products of Portland cement mortars

C. Famy[a,*], K.L. Scrivener[a], A. Atkinson[b], A.R. Brough[c]

[a]*Lafarge, Laboratoire Central de Recherche, 38291 Isle d'Abeau, France*
[b]*Materials Department, Imperial College, London, SW7 2BP, UK*
[c]*CEMU, Departments of Civil Engineering and Materials, University of Leeds, Leeds, LS2 9JT, UK*

Received 14 December 2000; accepted 20 August 2001

**Abstract**

The influence of both early and late heat treatments on the microstructure and on the hydration products of Portland cement mortars has been investigated. The mortars were given either a 4-h or 28-day precure at 20 °C before heating at 90 °C for 12 h and were subsequently stored in distilled water at 20 °C. The microstructure, studied by backscattered electron (BSE) imaging, shows the formation of distinct rims of inner C-S-H with different grey levels during the different stages of the curing cycles. The grey levels and corresponding BSE coefficients of these different rims were determined by image analysis and their chemical compositions by EDS microanalysis. It was found that the compositions depend on the temperature and time at which the rims had developed. The lighter C-S-H formed at 90 °C was denser and contained much more sulfate than the darker C-S-H formed at 20 °C, especially when the heat cure took place at early ages. The sulfate incorporated within the lighter C-S-H was released gradually over time. 

*Keywords:* Grey levels; Backscattered electron imaging; Backscatter electron coefficients; Two-tone C-S-H; Heat treatment

## 1. Introduction

The use of heat curing is widespread in the precast industry to accelerate strength development and thus allow rapid production of concrete components. Such increases in the early strengths and rate of hydration are associated with a modification of the microstructure: they have a coarser pore structure [1–4] and the rims of C-S-H formed around the cement grains are brighter relative to pastes cured at lower temperatures [2,5–8]. These rims of C-S-H are usually referred to as ''inner'' C-S-H as they are within the original boundaries of cement grains, as opposed to the outer C-S-H gel formed in the initially water-filled space [9].

This change in the inner C-S-H brightness was first observed in backscattered electron (BSE) images by Kjellsen et al. [2,5] on pastes hydrated at 50 °C, which exhibited brighter and thicker rims of inner C-S-H than did pastes hydrated at 5 or 20 °C. It was estimated that the thickness of the C-S-H rims in 28-day-old pastes increased from 5 μm at 20 °C to 25 μm at 80 °C [7].

In pastes hydrated at 80 °C and subsequently stored in water at 20 °C, Scrivener [8] and Scrivener and Taylor [10] observed cement grains surrounded by inner C-S-H of two distinct grey levels (tones): a lighter C-S-H rim formed at high temperature, inside which was a darker C-S-H rim developed during subsequent storage at 20 °C. The analysis totals of the lighter inner C-S-H were found to be higher (74–78%) than those of the darker inner C-S-H (57–64%) in 35-day-old pastes.

Higher sulfate concentrations have also been widely reported in C-S-H formed at temperatures above 60 °C [4,10–12].

The aim of the work described here was to examine the effect of precuring time before heating starts on the microstructure, analysis totals, BSE coefficients and chemical composition of inner C-S-H formed in mortars subjected to a short period of curing at 90 °C.

* Corresponding author. Tel.: +44-474828125; fax: +44-474828011.
*E-mail address*: charlotte.famy@pole-technologique.lafarge.com (C. Famy).

0008-8846/02/$ – see front matter 
PII: S0008-8846(01)00670-6

### 1.1. Origins of grey level contrast in BSE images

The atomic number is the principal factor determining grey level contrast in BSE images. More precisely, it has been established that (in the absence of other effects) the grey level is directly proportional to the backscatter coefficient $\eta$, which is related to the atomic number by the empirical equation [13]:

$$\eta = -0.0254 + 0.016Z - 1.86\times10^{-4}Z^2 + 8.3\times10^{-7}Z^3$$

When the specimen contains more than one element, the backscatter coefficient $\eta$ follows a simple rule of mixtures based on mass fractions:

$$\eta_{\text{mixture}} = \Sigma\eta_i C_i$$

where $i$ denotes each constituent, $\eta_i$ is the pure-element backscatter coefficient, $C_i$ is the mass fraction and the summation is taken over all constituents.

Consequently, the phases with the highest average atomic number will have the highest backscatter coefficient and will appear brightest in the image. Therefore, the typical constituents of a mortar can be distinguished by their grey values: anhydrous phases appear bright, calcium hydroxide (CH) light grey, C-S-H grey and porosity black. When phases are intermixed on a scale finer than the interaction volume for the BSEs, these phases cannot be distinguished in the image, where such regions have intermediate grey levels. Therefore, the presence of other phases intermixed with the analysed phase affects the backscatter coefficient.

Theoretically, the backscatter coefficient should not be affected by the density with which the atoms are packed or by microporosity where this is significantly finer than the interaction volume. When the density is lower, the mean free path of the incoming electrons will increase and BSEs will be produced over a wider volume, but on average, the total number of BSE should not change. However, it has been found that microporosity does in fact affect the grey levels observed in BSE images [8,14]. The reasons for this are not well established, but it is probably related to the fact that solid-state backscattered detectors, commonly used in scanning electron microscopy (SEM), only detect the BSEs generated over a certain solid angle close to the incoming beam. Thus, if the same number of BSEs is generated over a wider volume, less will be detected by the detector.

For C-S-H gel, the effective density or microporosity in the high vacuum of the SEM will also depend on its water content in the saturated state. In this paper, the term density is used loosely to describe the combined effects of microporosity and water content in the saturated state.

### 1.2. Factors affecting microanalysis totals

For microanalyses in which a constant beam current is used and which are calibrated against standards, without normalisation, the analysis totals correspond to the sum of the elements detected. Even for thin-window or windowless detectors, quantitative analysis for elements below sodium is not very reliable, and the lighter elements are generally excluded from the analysis. For phases containing oxides, the amount of oxygen present is usually calculated by stoichiometry and added to the analysis total. Therefore, for cementitious materials, the principal origin of a shortfall in analysis totals is the water and carbonate contents, as hydrogen cannot be detected by X-ray microanalysis and carbon cannot be quantified.

When microanalyses are performed on anhydrous cement grains, the analysis totals are very close to the theoretical 100% value because such phases do not contain water. Similarly, microanalyses of CH deposits give analysis totals around the theoretical value of 76%, the difference from 100% resulting from water content. For C-S-H, values around 76% are commonly obtained [6,8,14,15]. The deficit of 24% is much more than can reasonably be attributed to the water present in the C-S-H exposed to the high vacuum of the instrument [14,16]. Consequently, it must be supposed that the analysis totals for C-S-H are also affected by the presence of microporosity, either that present in the saturated state or that created by drying in the high vacuum. Such an assumption is supported by the experimental findings of Harrison et al. [14] and Kjellsen and Helsing Atlassi [15]. A correlation between the analysis totals and the local capillary porosity showed that the analysis totals decreased as the local porosity increased [15]. The effects may be due to retardation of the incident electrons by fields resulting from internal charging on the surfaces of the pores [14], but further investigations on their origin are required.

## 2. Experimental

The mortar specimens were prepared using an ordinary Portland cement (65.5% CaO, 21.9% $SiO_2$, 5.4% $Al_2O_3$, 2.2% $Fe_2O_3$, 1.1% $K_2O$, 0.1% $Na_2O$, 1.3% MgO, 3.9% $SO_3$). The siliceous aggregate was the German Normensand standard DIN EN 196-1. Mortar prisms were cast in $16 \times 16 \times 160$-mm$^3$ moulds using a water/cement ratio of 0.5 and sand/cement ratio of 3. After casting, the mortar specimens were given either a 4-h or 28-day precure (Regimes 2 and 3, respectively, in Fig. 1). During the precure, they were kept in the moulds in a saturated atmosphere at 20 °C. The temperature was then increased at a rate of 30–35 °C/h to 90 °C which was maintained for 12 h. At the end of the heat treatment, the prisms were allowed to cool naturally to 20 °C over approximately 5 h. They were then demoulded and subsequently stored in distilled water at 20 °C. A mortar cured at 20 °C for 24 h and subsequently demoulded and stored in water for 300 days served as a reference (Regime 1 in Fig. 1).

The specimens for examination were first freeze dried to stop further hydration at selected times (Fig. 1). They were then vacuum impregnated with epoxy-resin, lapped to a flat

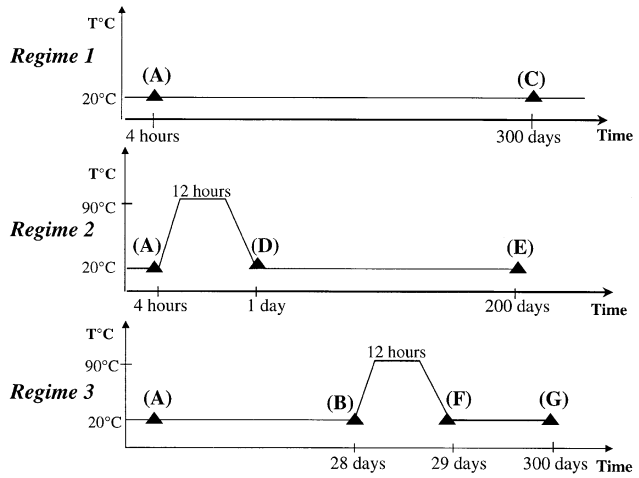


Fig. 1. Curing regimes applied to mortars: *Regime 1* for 20 °C cure, *Regime 2* for 4-h precure followed by a 90 °C heating for 12 h and *Regime 3* for 28-day precure followed by a 90 °C heating for 12 h. The triangle symbols correspond to the time at which mortars were freeze dried to allow SEM examination. The letters in brackets give the order at which specimens are discussed.

surface with 9 μm alumina and polished successively with 3, 1 and 1/4 μm diamond paste. A carbon coating was applied to the polished sections for study by SEM using a JEOL JSM 35-CF equipped with a solid-state BSE detector and a PGT/IMIX energy dispersive X-ray (EDX) analyser. The microscope was operated at an accelerating voltage of 15 kV. The EDX system had computer software allowing ZAF corrections to be automatically performed, and micro-analyses were standardised with suitable pure phases (e.g. wollastonite for calcium and silicon). Analyses of pure clinker phases (e.g. $C_3S$ and $C_3A$) were made frequently to check beam current and to verify the accuracy of the calibration and computational procedures. Oxygen was calculated by stoichiometry on the basis of the other elements present.

BSE image analysis was used to determine the grey values (brightness) of each type of C-S-H. The BSE images contained $512 \times 512$ pixels with 256 grey levels. For each image, a histogram representing the frequency of pixels as a function of the grey level (0–255) was generated. The histogram exhibits peaks corresponding to the individual phases. The grey values of the C-S-H products were calculated by interpolation between two phases with known and distinct backscatter coefficients; $C_3S$ (from anhydrous cement grains) and quartz (from aggregates) were selected.

The grey values for $C_3S$, quartz and C-S-H were taken as the maxima of their peaks in the histogram. As the difference in the backscatter coefficients of $C_3S$ and quartz is proportional to the difference in their grey values, the difference in the backscatter coefficients of $C_3S$ and C-S-H will be similarly proportional to the difference in their grey values. This method was used for all the specimens to calculate the backscatter coefficient of the C-S-H products. Care must be taken when determining the C-S-H grey value because of the diffuse boundaries between the zones of C-S-H formed at different temperatures and because (unlike $C_3S$ or quartz, which have distinct grey levels) the C-S-H tends to have a range of grey values due to its microporosity. When it was difficult to differentiate the boundaries between the zones of C-S-H formed at different temperatures, the histograms for smaller areas were plotted and studied as described above. Values for 10 areas were averaged to calculate each of the backscatter coefficients.

## 3. Results and discussion

### 3.1. Microstructural observations

#### 3.1.1. 4 h at 20 °C (Point A, Fig. 1)

After 4 h of hydration at 20 °C, very little hydration has occurred as indicated by the preponderance of unreacted cement grains and the large degree of porosity (Fig. 2). Very little inner C-S-H has started to form around the anhydrous particles, although some outer C-S-H gel has precipitated throughout the structure. It is not possible to identify any ettringite crystals in the BSE images, although a small peak was detected by X-ray diffraction [12]. This suggests that, at this very early stage of hydration, ettringite is embedded within C-S-H products as previously reported by Scrivener and Taylor [10] and as observed by Scrivener [17] in TEM images of young cement pastes. Masses of CH are observed throughout the paste.

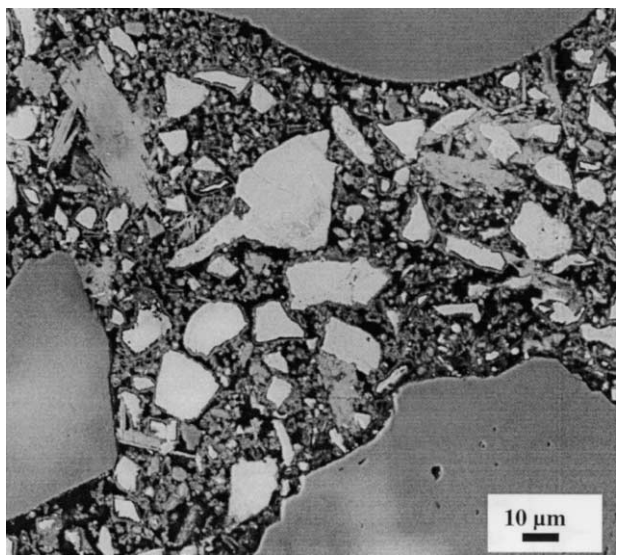


Fig. 2. BSE image of the mortar precured for 4 h at 20 °C (Point A, Fig. 1). Very little hydration has occurred at this stage as indicated by the very thin hydration rims starting to form around cement grains.

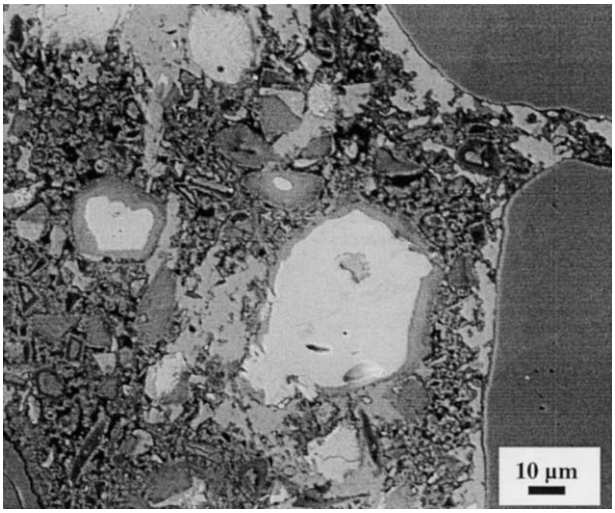


Fig. 3. BSE image of the mortar precured for 28 days at 20 °C (Point B, Fig. 1).

*3.1.2. 28 days at 20 °C (Point B, Fig. 1)*

After 28 days at 20 °C, the specimen displays the characteristic microstructural features widely observed in mortars cured at room temperature, with thick rims of inner C-S-H surrounding the cement grains together with masses of CH in the originally water occupied space (Fig. 3). In some of the more porous areas, ettringite crystals can be identified at higher magnifications.

*3.1.3. 300 days at 20 °C (Point C, Fig. 1)*

After 300 days at 20 °C, the microstructure is denser, with less porosity (Fig. 4). The rims around the alite in the cement grains are thicker and have a fairly even grey level. At higher magnifications, deposits of both ettringite and calcium monosulfoaluminate were observed within the structure.

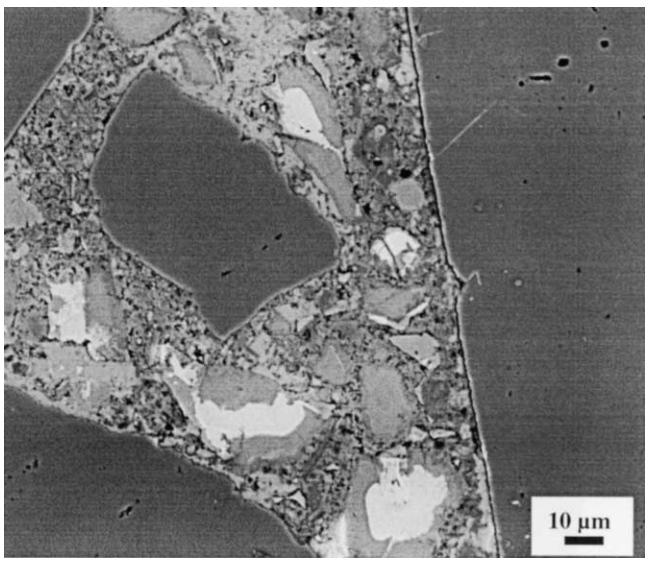


Fig. 4. BSE image of the 20 °C cured mortar stored in water for 300 days (Point C, Fig. 1). Thick one-tone rims of C-S-H have developed around alite grains. Fully hydrated alite grains can be observed.

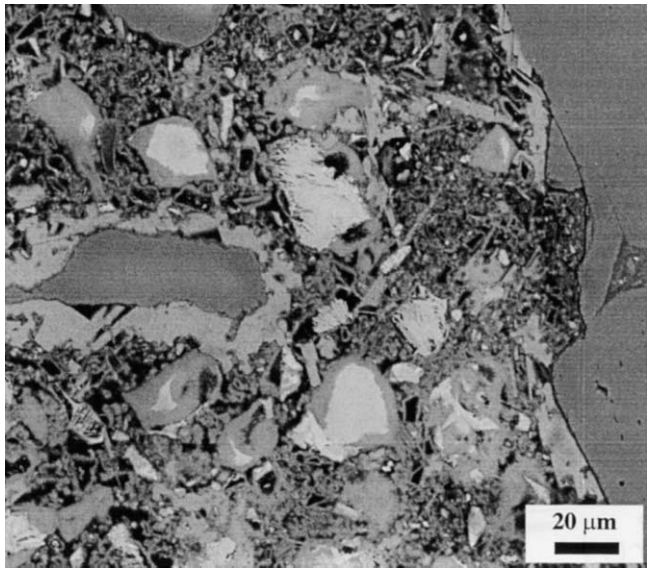


Fig. 5. BSE image of the 4-h precured mortar directly after heating at 90 °C (Point D, Fig. 1). Thick rims of inner C-S-H surround alite grains.

*3.1.4. Mortar precured for 4 h at 20 °C then heated at 90 °C for 12 h (Point D, Fig. 1)*

Fig. 5 shows the microstructure of the mortar cured for 12 h at 90 °C after a 4-h precure at 20 °C. The accelerating effect of temperature on the hydration reaction is apparent, with C-S-H rims some 3–4 μm thick surrounding the cement grains. The smallest cement grains have completely

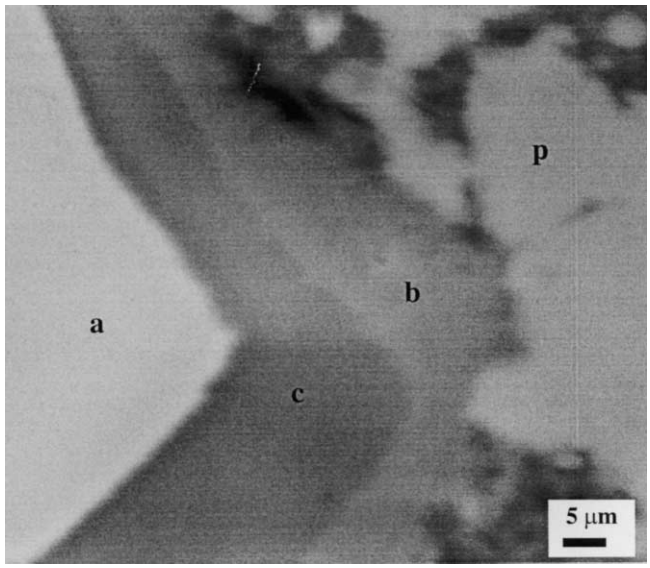


Fig. 6. BSE image of the 4-h precured mortar heated at 90 °C for 12 h and subsequently stored in water for 200 days (Point E, Fig. 1). The alite grain (a) is rimmed by two-tone inner C-S-H: the lighter (b) early C-S-H formed at 90 °C and the post-cured darker C-S-H (c). (p) is a deposit of portlandite.

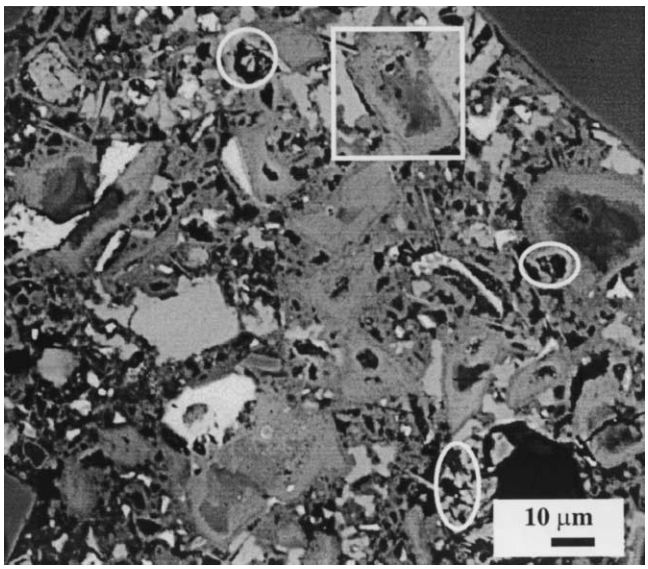


Fig. 7. BSE image of the 4-h precured mortar heated at 90 °C for 12 h and subsequently stored in water for 200 days (Point E, Fig. 1). Two-tone inner C-S-H have formed (square). Ettringite is observed (ovals) in air voids, cavities and also within the $C_4AF$ original boundaries.

hydrated to leave hollow shells of hydration products. Deposits of calcium monosulfoaluminate infilling pores could be found dispersed throughout the microstructure. There was no sign of ettringite crystals, whose absence was confirmed by X-ray diffraction and NMR studies reported elsewhere [12].

*3.1.5. Mortar precured for 4 h at 20 °C then heated at 90 °C for 12 h and subsequently stored in water for 200 days at 20 °C (Point E, Fig. 1)*

In this specimen, the rims of C-S-H surrounding the unhydrated cores of the cement grains exhibit two distinct grey levels (Fig. 6). The exterior rim is lighter than the darker interior one adjacent to the anhydrous cement core. By comparison with the preceding specimen, it is clear that the lighter C-S-H is that which was formed during the period at elevated temperature (90 °C), while the darker C-S-H has been formed during the subsequent storage in water at 20 °C. This darker C-S-H is hereafter referred to as *post-cured darker C-S-H*.

Some cement grains have totally reacted, leaving a rim of lighter C-S-H filled with a core of post-cured darker C-S-H (Fig. 7). Clusters of ettringite crystals are observed within the structure (Fig. 7) instead of the calcium monosulfoaluminate deposits detected directly after the heat curing. They appear dark grey and have a cracked aspect due to drying during specimen preparation. At this stage, the paste is dense with a low porosity.

The microstructural development observed in the 4-h precured mortars is schematically represented in Fig. 8.

*3.1.6. Mortar precured for 28 days at 20 °C then heated at 90 °C for 12 h (Point F, Fig. 1)*

Around the larger cement grains, which had not completely hydrated at 28 days, a lighter rim of C-S-H has formed at the higher temperature inside the darker one already present after 28 days at 20 °C (Figs. 9 and 10). Thus, two-tone rims have been formed in which the contrast is the inverse of that observed in the rims formed by early heat curing and subsequent moist storage at 20 °C. The darker C-S-H rim has first developed around the alite grain during the 28 days at 20 °C and is defined as the *pre-cured darker C-S-H*. The lighter C-S-H is formed later, while the mortars are cured at 90 °C.

Some other plate-like crystals are observed in the paste and identified as calcium monosulfoaluminate (Fig. 10). No ettringite crystals are detected.

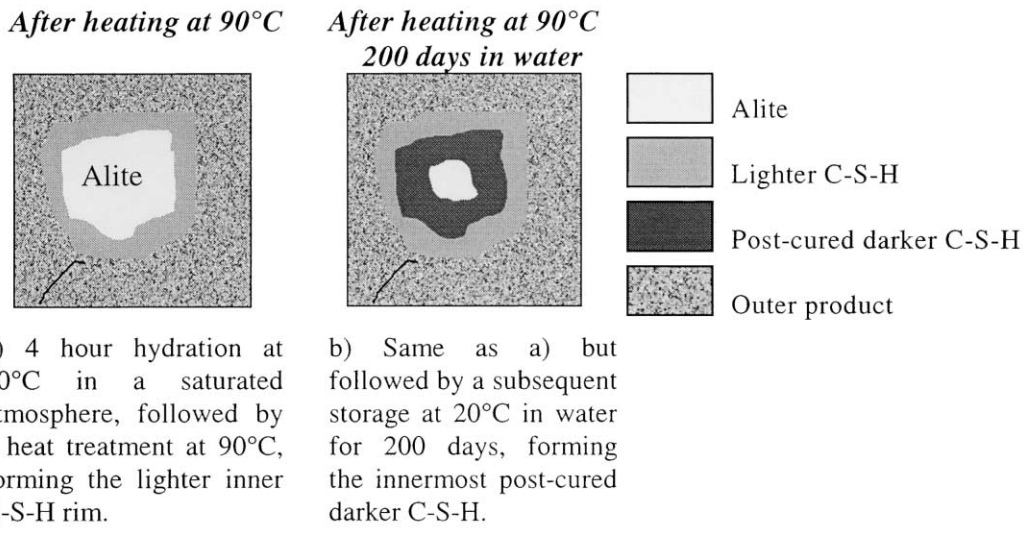


Fig. 8. Microstructural development of the two-tone C-S-H in the 4-h precured mortars.

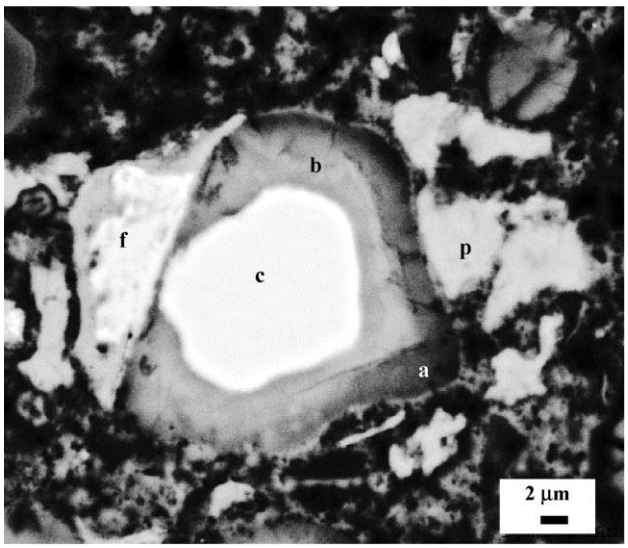


Fig. 9. High-magnification BSE image of the 28-day precured mortar directly after heating at 90 °C for 12 h (Point F, Fig. 1). The pre-cured darker C-S-H (a) and lighter C-S-H (b) rims have formed around an alite grain (c). (p) is portlandite and (f) is remaining unreacted, interstitial ferrite phase.

*3.1.7. Mortar precured for 28 days at 20 °C then heated at 90 °C for 12 h and subsequently stored in water for 300 days at 20 °C (Point G, Fig. 1)*

After storage in water for 300 days, the alite of the remaining reacted cement grains have further hydrated to form an inner *postcured* darker C-S-H so that now three types of C-S-H are observed in the largest cement grains. The *postcured darker C-S-H* has developed inside the two previously discussed rims of *lighter* and *precured darker C-S-H* (Fig. 11). The postcured darker C-S-H appears slightly darker than the precured darker C-S-H. Some clusters of ettringite exhibiting a characteristic cracked appearance are distributed within the paste. No calcium monosulfoaluminate was observed.

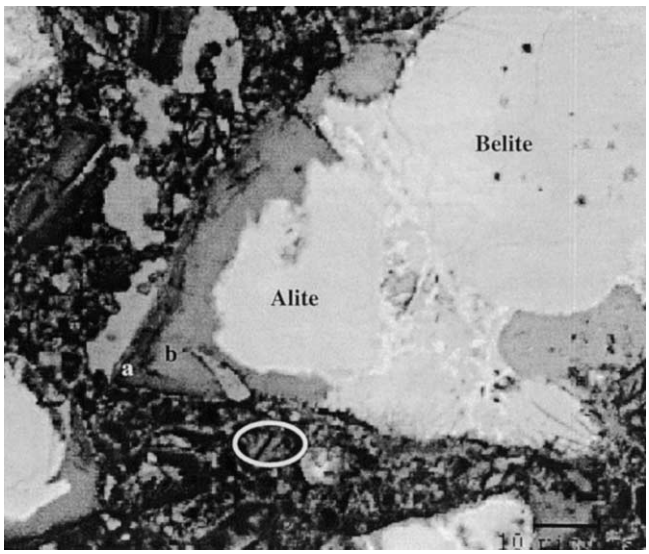


Fig. 10. BSE image of the 28-day precured mortar heated at 90 °C for 12 h (Point F, Fig. 1). A polymineralic clinker grain is shown containing ferrite (very bright), alite and belite. The pre-cured darker (a) and lighter C-S-H (b) rims are seen surrounding the alite grain calcium monosulfoaluminate was also found (oval).

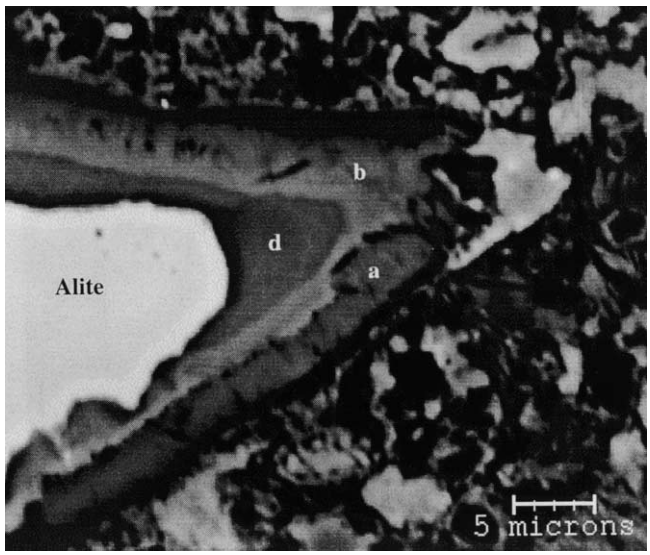


Fig. 11. BSE image of the 28-day precured mortar stored in water for 300 days (Point G, Fig. 1) showing the three rims of pre-cured (a), lighter (b) and post-cured darker C-S-H (d) surrounding the alite grain.

The microstructural development observed in the heat cured mortars, precured for 28 days, is shown schematically in Fig. 12.

*3.2. Microanalyses of the inner C-S-H products*

The EDS microanalyses were carried out on the C-S-H rims (pre-cured darker, lighter C-S-H and post-cured darker rims). For statistical accuracy, about 25 point microanalyses were acquired for each specimen, each in a distinct individual rim.

*3.2.1. Mortars cured at 20 °C (Points B and C, Fig. 1)*

No microanalyses are reported for the mortars cured at 20 °C for only 4 h as the rims are much thinner than the interaction volume for microanalyses at this age.

The S/Ca and Al/Ca atomic ratios of the inner C-S-H in the mortar cured at 20 °C and subsequently stored for 28 days in a saturated atmosphere or in water for 300 days are shown in Fig. 13. The microanalyses are spread over a large range of S/Ca and Al/Ca values. Such variations suggest the presence of other phases intimately mixed within the inner C-S-H gel with a particle size too small to be resolved by the microprobe (less than about 1 μm). The microanalyses are compatible with mixtures of C-S-H containing small amounts of $SO_3$ and $Al_2O_3$ with ettringite, which has a S/Ca ratio of 1.5, although a little calcium monosulfoaluminate might also be present. Table 1 includes estimated values of the atomic ratios of the C-S-H components. The Al/Ca

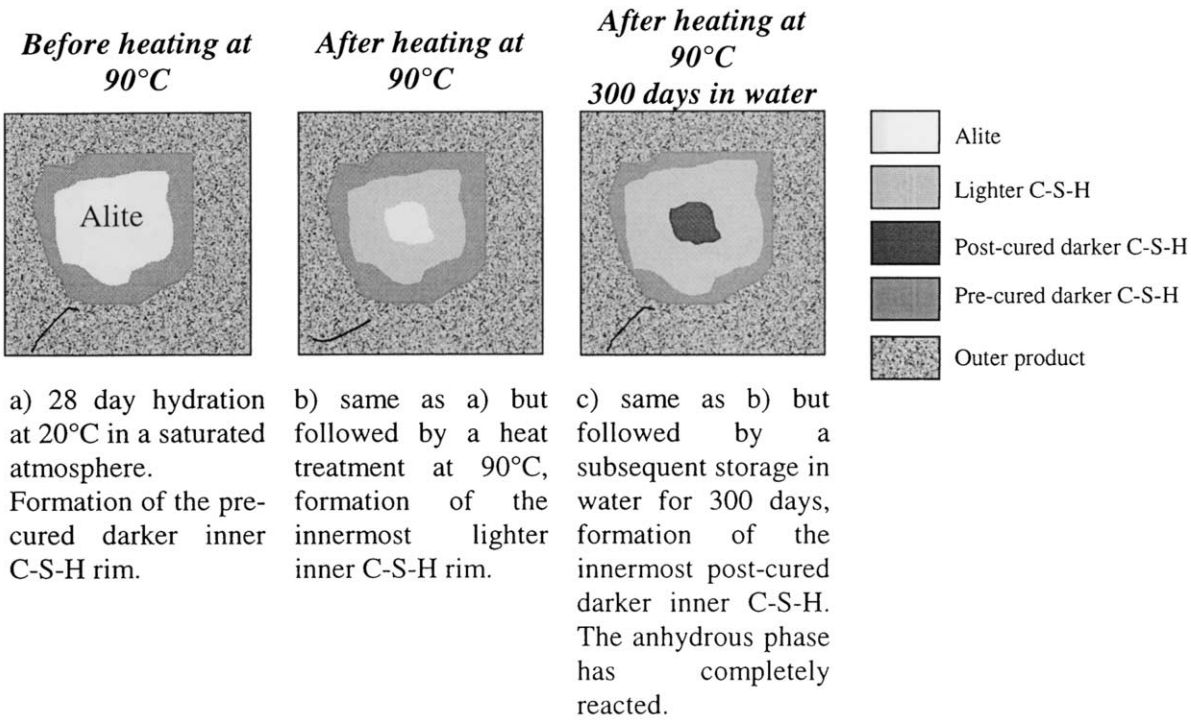


Fig. 12. Microstructural development of the three-tone C-S-H in the 28-day precured mortars.

ratios of the C-S-H (around 0.04) are similar to those found by Richardson et al. [18]. The small decrease in the S/Ca and Al/Ca ratios with time can possibly be attributed to a dilution effect, because any increases in the amounts of available $SO_4^{2-}$ and $Al^{3+}$ are small relative to that of C-S-H.

*3.2.2. Lighter inner C-S-H in the 4-h and 28-day precured mortars directly after heating and after subsequent storage in water (Points D–G, Fig. 1)*

After heating at 90 °C, the 4-h precured mortars give lighter C-S-H with higher S/Ca ratios and, to a lesser extent, higher Al/Ca ratios than the 28-day precured mortars (Fig. 14).

During subsequent storage in water, the Al/Ca ratios of the lighter C-S-H show only small changes (Fig. 14 and Table 1). It has been shown by NMR and microanalyses in the TEM that some Al is present in the C-S-H substituting Si [12,18] and it is likely that this occurs in the lighter C-S-H. The difference in charge between $Al^{3+}$ and $Si^{4+}$ is most probably balanced by a proton $H^+$. The mean Al/Si ratio of the inner C-S-H for all the mortars was 0.10 (Table 1), which is similar to the values found by Richardson et al. [18].

A significant decrease in the S/Ca ratios of both mortars occurs during subsequent storage in water. The loss of sulfate from the lighter C-S-H is much faster in the 4-h precured mortars than in the 28-day precured mortars.

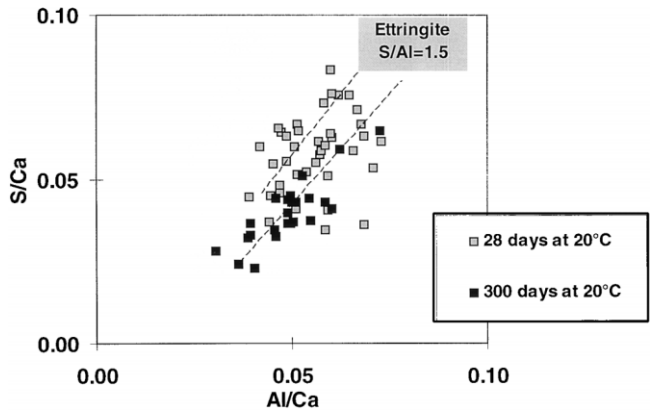


Fig. 13. S/Ca atomic ratios vs. Al/Ca atomic ratios for the inner C-S-H of the 20 °C cured mortars stored 28 or 300 days without heat cure (Points B and C, Fig. 1).

Table 1
Atomic ratios, analysis totals (%) and BSE coefficients of the different-tone C-S-H before and after heating

| | Atomic ratios | | | | In C-S-H per 1 Ca total | | | | | |
|---|---|---|---|---|---|---|---|---|---|---|
| | S/Ca | Al/Ca | Si/Ca | Al/Si | Ca | Si/Ca | Al/Ca | (Si + Al)/Ca | Analysis total (%) | BSE coefficient |
| **20 °C cured mortar** | | | | | | | | | | |
| 20 °C/28 days | 0.050 | 0.045 | 0.494 | 0.129 | 0.950 | – | – | – | 67 | 0.139 |
| 20 °C/300 days | 0.030 | 0.040 | 0.494 | 0.095 | 0.970 | – | – | – | 74 | 0.140 |
| **4 h (pre)/90 °C for 12 h** | | | | | | | | | | |
| After heating (L) | 0.070 | 0.061 | 0.468 | 0.121 | 0.930 | 0.503 | 0.066 | 0.569 | 80 | 0.143 |
| 200 days (L) | 0.016 | 0.046 | 0.507 | 0.089 | 0.984 | 0.515 | 0.047 | 0.562 | 72 | 0.141 |
| 200 days (PostD) | 0.006 | 0.053 | 0.543 | 0.097 | 0.994 | 0.546 | 0.053 | 0.600 | 60 | 0.132 |
| **28 days (pre)/90 °C for 12 h** | | | | | | | | | | |
| After heating (PreD) | 0.047 | 0.050 | 0.535 | 0.089 | 0.953 | 0.561 | 0.052 | 0.614 | 60 | 0.131 |
| After heating (L) | 0.056 | 0.050 | 0.513 | 0.092 | 0.944 | 0.543 | 0.053 | 0.596 | 80 | 0.142 |
| 300 days (PreD) | 0.027 | 0.046 | 0.538 | 0.083 | 0.973 | 0.553 | 0.047 | 0.600 | 60 | 0.129 |
| 300 days (L) | 0.039 | 0.047 | 0.509 | 0.088 | 0.961 | 0.530 | 0.049 | 0.579 | 73 | 0.140 |
| 300 days (PostD) | 0.029 | 0.046 | 0.500 | 0.089 | 0.971 | 0.515 | 0.047 | 0.562 | 59 | 0.132 |

The numbers represent the mean value of at least 25 X-ray microanalyses with a standard error of 0.002 for the atomic ratios and BSE coefficients and 0.5% for analysis totals. Abbreviations: L for lighter C-S-H, pre for precure, PreD for pre-cured darker C-S-H and PostD for post-cured darker C-S-H.

The EDS microanalyses do not give any information about the nature of the interactions between sulfate and lighter C-S-H. Earlier Kalousek [19] and later Copeland et al. [20] suggested that $SO_4^{2-}$ substituted for Si. However, the easy release of sulfate from the lighter C-S-H during subsequent storage indicates that the sulfate is unlikely to be chemically bound in the lighter C-S-H structure but is either adsorbed or absorbed. This conclusion agrees with that based on studies of synthetized C-S-H or $C_3S$ pastes [21–23]. The decrease in S/Ca ratios after subsequent storage is associated with an increase in the Si/Ca ratios (Table 1). This suggests that sorbed $SO_4^{2-}$ is balanced by sorbed $Ca^{2+}$ in the lighter C-S-H.

Knowing the Si/Ca, S/Ca and Al/Ca ratios of the C-S-H and assuming that the C-S-H contains Si partly replaced by Al and that sorbed $SO_4^{2-}$ is charged balanced by sorbed $Ca^{2+}$, it is possible to calculate the amounts of Ca integral to the C-S-H structure (not present as $CaSO_4$). The Si/Ca and Al/Ca ratios in the C-S-H can then be given relative to these latter values (Table 1). The results suggest a mean (Si + Al)/Ca in the C-S-H approximately constant at 0.58 (Ca/(Si + Al) = 1.71), which is similar to what is found in the C-S-H of a $C_3S$ or $C_2S$ paste. This is also consistent with the hypothesis that Al substitutes for Si in the C-S-H.

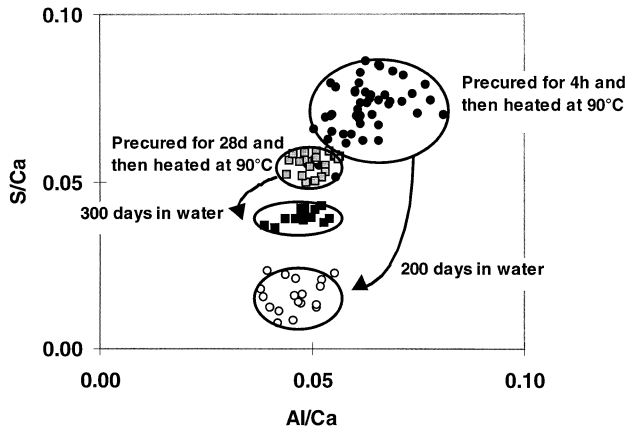


Fig. 14. S/Ca atomic ratios vs. Al/Ca atomic ratios for the lighter inner C-S-H of the 4-h and 28-day precured mortars, after heating at 90 °C and after a subsequent storage in water at 20 °C (Points D–G, Fig. 1).

### *3.2.3. Post-cured darker inner C-S-H of the 4-h and 28-day pre-cured mortars after subsequent storage in water (Points E and G)*

The post-cured darker C-S-H, formed after heating and during subsequent storage at 20 °C, exhibited lower S/Ca ratios than the lighter C-S-H (Table 1). This shows that even after an extended period of storage in water, the content of sulfate incorporated within the lighter C-S-H was still a key discriminating parameter between the C-S-H formed at 90 °C and that formed at 20 °C. The former had a greater affinity for sulfate than the latter.

## *3.3. Analysis totals and backscatter coefficients*

It is important to note that the materials studied have all been subject to dehydration occurring during freeze drying and specimen preparation, resulting in increased microporosity and a consequent decrease in the analysis totals (Table 1).

The plot of the BSE coefficients against analysis totals shows a fairly high correlation (not necessary linear), which suggests that both measure the same thing (Fig. 15). Three groups may be distinguished on that plot:

1. Analysis totals of approximately 70% for the C-S-H in the samples cured at 20 °C and for the lighter C-S-H after storage in water at 20 °C.
2. Analysis totals of 80% for the lighter C-S-H formed at 90 °C and examined directly after heating.

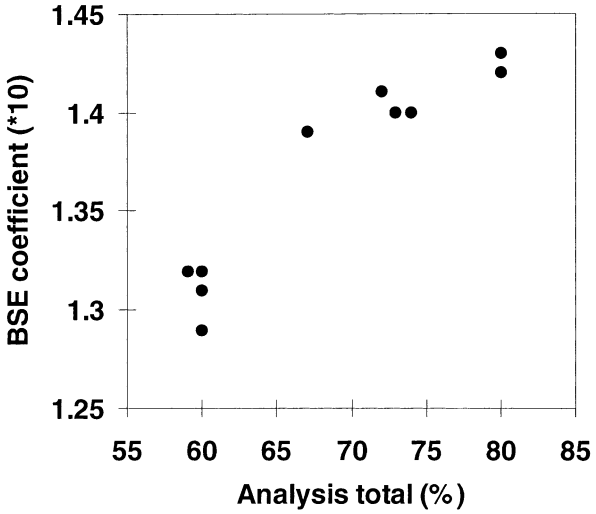


Fig. 15. BSE coefficients ( × 10) vs. analysis totals for the pre-cured, lighter and post-cured darker C-S-H.

3. Analysis totals of 60% for the C-S-H formed on 28-day precure and then heated at 90 °C and also the post-cured darker C-S-H developed on storage in water at 20 °C after heating.

The analysis totals for the C-S-H of the samples cured at 20 °C and for the lighter C-S-H present after storage in water at 20 °C are similar to those reported previously [6,8,14,15]. As noted earlier, they are too low for the deficits from 100% to be attributable purely to the water content. For C-S-H as it exists in the high vacuum, this is probably similar to that of D-dried sample of the same Ca/Si ratio [9]. The most probable composition is therefore approximately $1.7CaO{\cdot}SiO_2{\cdot}1.4H_2O$, for which the backscatter coefficient would be 0.151 and the analysis total 86%. The microporosity that is indicated by the low total and the corresponding backscatter coefficient presumably includes any that is present in the undried or partly dried material but will be augmented by that replacing the water that is lost during specimen preparation and examination in the SEM.

The values of analysis totals for the lighter C-S-H present directly after heating at 90 °C are higher than those of the C-S-H in samples cured at 20 °C or for the lighter C-S-H cured at 90 °C and subsequently stored at 20 °C, but they, too, are lower than those corresponding to the formula $1.7CaO{\cdot}SiO_2{\cdot}1.4H_2O$. As noted earlier, among the three parameters, which may affect analysis totals, the presence of other phases intermixed within the C-S-H on a submicrometre scale is one of them. If intermixed phases were responsible, this should be related to the sulfate content as this is the most significant difference between the lighter C-S-H after heating and the other inner C-S-H. The presence of sulfate could contribute to the increased brightness. However, a S/Ca ratio of 0.070 in the lighter C-S-H of the 4-h precured mortars corresponds to an $SO_3$ content of 4.7% (wt) (out of an analysis total of 80%), and such a small amount of $SO_3$ would have increased the average backscatter coefficient by only 0.001, which would not have a noticeable effect. Furthermore, the backscatter coefficients do not correlate with the mean S/Ca ratios of the C-S-H (Fig. 16), suggesting that the sulfate has a minimal effect. This shows that the pore structure of the C-S-H formed at 90 °C and examined directly after heating differs from that of the C-S-H cured at 20 °C. The water content of the C-S-H as it exists in the SEM could be the same as in the two cases, but there is less microporosity in the lighter C-S-H formed at 90 °C. The lighter C-S-H may have contained less microporosity before it was dried. In addition, it probably contained less water before it was dried, which would decrease the contribution to the microporosity that occurred on drying.

The low analysis totals of the third group (60%) are difficult to explain, especially for the post-cured darker C-S-H formed on storage at 20 °C after heating. They suggest a higher fine porosity, a higher amount of interlayer space initially filled with water before sample preparation or both. The reasons for the difference from the C-S-H formed at 20 °C in non-heated mortars (74%) are, however, not clear. The only other difference between the post-cured darker C-S-H and the C-S-H in 20 °C cured mortars lies in their microstructural context, i.e. the post-cured darker C-S-H is surrounded by a rim of lighter C-S-H.

## 4. Relation to expansion

Linear expansion measurements were carried out in parallel on the specimens. The results, reported elsewhere [12,24], show that the 28-day precured mortars do not expand following heat curing at 90 °C, whereas the 4-h precured mortars do. The different expansive behaviours

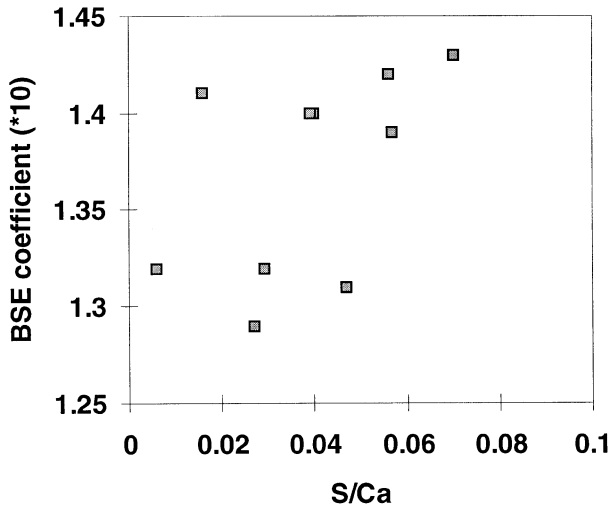


Fig. 16. BSE coefficients ( × 10) vs. mean S/Ca atomic ratios for the pre-cured, lighter and post-cured darker C-S-H.

can be explained by the different amounts of C-S-H formed at 90 °C. Following the 28-day precure at 20 °C, most of the C-S-H had formed at 20°C. Therefore, heat treatment has less influence than in the mortars precured for only 4 h.

## 5. Conclusions

- The influence of an early and a late heat treatment at 90 °C on the microstructure and composition of inner C-S-H products has been studied. Directly after the heat cure, the BSE images of the 28-day precured mortars exhibit residual alite grains rimmed with two-tone C-S-H: a pre-cured darker C-S-H rim surrounding a lighter C-S-H rim. The darker rim was developed during the precure for 28 days and the lighter formed at 90 °C. After subsequent storage in water at 20 °C, the alite grains have been further hydrated to a post-cured darker C-S-H and the BSE images present a three-tone inner C-S-H. Thus, the inner C-S-H products formed during precuring at 20 °C, heat curing at 90 °C and subsequent storing at 20 °C can be distinguished by their grey levels.
- EDS microanalyses have shown that the chemical compositions of the different C-S-H rims depend mainly on the temperature at which they were formed. The lighter C-S-H, which was formed at 90 °C, can have a greater affinity with respect to sulfate than the C-S-H developed at 20 °C (pre or post-cured C-S-H products). During subsequent storage at 20 °C, the release of sulfate from the lighter C-S-H gel indicates that $SO_4^{2-}$ is not chemically bound in the C-S-H structure but may only be sorbed and balanced by sorbed $Ca^{2+}$ in the C-S-H during heat curing. The calculated (Si + Al)/Ca ratios were consistent with the assumption that $Al^{3+}$ substitutes for $Si^{4+}$ in the inner C-S-H (the difference in charge between $Al^{3+}$ and $Si^{4+}$ probably being balanced by a proton $H^+$).
- A fairly good correlation was found between the analysis totals and the backscatter coefficients. The differences in the analysis totals and in the backscatter coefficients of the C-S-H rims were found to be independent of the sulfate level and probably give indications of relative porosity and water content. However, more work is needed to explain the influence of microporosity and water contents on the analysis totals.

## Acknowledgments

The authors thank Prof. H.F.W Taylor for his helpful comments, Drs. D. Sorrentino and P. Barriac for their discussions and the UK Engineering and Physical Sciences Research Council for assistance with purchase of the microanalysis equipment (grant number GR/L-26537).

## References

[1] G.J. Verbeck, R.H. Helmuth, Proceedings of the 5th ICC, Vol. 1, Tokyo, 1968.
[2] K.O. Kjellsen, R.J. Detwiler, O.E. Gjorv, Backscattered electron imaging of cement pastes hydrated at different temperatures, Cem. Concr. Res. 20 (1990) 308–311.
[3] Y. Cao, R. Detwiler, Backscattered electron imaging of cement pastes cured at elevated temperature, Cem. Concr. Res. 25 (1995) 627–638.
[4] H.H. Patel, C.H. Bland, A.B. Poole, The microstructure of concrete cured at elevated temperatures, Cem. Concr. Res. 25 (1995) 485–490.
[5] K.O. Kjellsen, R.J. Detwiler, O.E. Gjorv, Development of microstructure in plain cement pastes hydrated at different temperatures, Cem. Concr. Res. 21 (1991) 179–189.
[6] K.O. Kjellsen, Heat curing and post heat curing regimes of high performance concrete: Influence on microstructure and C-S-H composition, Cem. Concr. Res. 26 (1996) 295–307.
[7] H.H. Patel, C.H. Bland, A.B. Poole, The microstructure of steam-cured precast concrete, Adv. Cem. Res. 8 (29) (1996) 11–19.
[8] K.L. Scrivener, The effect of heat treatment on inner product CSH, Cem. Concr. Res. 22 (1992) 1224–1226.
[9] H.F.W. Taylor, in: T. Telford (Ed.), Cement Chemistry, second ed., Telford, London, 1997.
[10] K.L. Scrivener, H.F.W. Taylor, Delayed ettringite formation: A microstructural and microanalytical study, Adv. Cem. Res. 5 (20) (1993) 139–146.
[11] M.C. Lewis, Heat curing and delayed ettringite formation in concretes, PhD thesis, Imperial College of Science, Technology and Medicine, University of London, UK, 1996.
[12] C. Famy, Expansion of heat-cured mortars, PhD thesis, Imperial College of Science, Technology and Medicine, University of London, UK, 1999.
[13] J.I. Goldstein, D.E. Newbury, P. Echlin, D.C. Joy, A.D Romig, C.E. Lyman, C. Fiori, E. Lifshin, Scanning Electron Microscopy and X-Ray Microanalysis, second ed., Plenum, New York, 1992.
[14] A.M. Harrison, N.B. Winter, H.F.W. Taylor, X-ray microanalysis of microporous materials, J. Mater. Sci. Lett. 6 (1987) 1339–1340.
[15] K.O. Kjellsen, E. Helsing Atlassi, X-ray microanalysis of hydrated cement: Is the analysis total related to porosity? Cem. Concr. Res. 28 (1998) 161–165.
[16] A.M. Harrison, N.B. Winter, H.F.W. Taylor, Proceedings of the 8th ICCC, Vol. 1, Rio, 1986, p. 82.
[17] K.L. Scrivener, The development of microstructure during the hydration of Portland cement, PhD Thesis, Imperial College of Science, Technology and Medicine, University of London, UK, 1984.
[18] I.G. Richardson, A.R. Brough, R. Brydson, G.W. Groves, C.M. Dobson, Location of aluminium in substituted calcium silicate hydrate (C-S-H) gels as determined by $^{29}Si$ and $^{27}Al$ NMR and EELS, Am. Ceram. Soc. 76 (9) (1993) 2285–2288.
[19] G.L. Kalousek, Analysing $SO_3$-bearing phases in hydrating cements, Mater. Res. Stud. 6 (1965) 292–304.
[20] L.E. Copeland, E. Bodor, T.N. Chang, C.H. Weise, Reactions of tobermorite gel with aluminates, ferrites, and sulfates, PCA Res. Dev. Lab. (1967) 61–75 (Jan).
[21] I. Odler, Interaction between gypsum and the C-S-H phase formed in $C_3S$ hydration, Proceedings of the 7th ICCC, Vol. 4, 195, pp. 493–495.
[22] Y. Fu, P. Xie, J.J. Beaudoin, Effect of the temperature on sulphate adsorption/desorption by tricalcium silicate hydrates, Cem. Concr. Res. 24 (1994) 1428–1432.
[23] L. Divet, R. Randriambololona, Delayed ettringite formation: The effect of temperature and basicity on the interaction of sulphate and C-S-H phase, Cem. Concr. Res. 28 (1998) 357–363.
[24] C. Famy, K.L. Scrivener, A.R. Brough, A. Atkinson, Influence of the length of pre-cure on expansion of heat-cured mortars, in preparation.